6.

The association of glucose metabolism and eigenvector centrality in Alzheimer's disease

S.M. Adriaanse, A.M. Wink, B.M. Tijms, R. Ossenkoppele, S. Verfaillie, A.A. Lammertsma, R. Boellaard, P. Scheltens, B.N.M. Berckel, F. Barkhof,

Submitted.

Abstract

Purpose Both [^{18}F]FDG PET, examining glucose metabolism, and resting-state fMRI (rs-fMRI), using co-varying blood-oxygen levels, can be used to explore neuronal dysfunction in Alzheimer's disease (AD). Both measures are reported to identify similar brain regions affected in AD patients. The spatial overlap and association of [^{18}F]FDG with rs-fMRI in AD patients and controls was examined in order to investigate whether and, if so, to what extent, these two measures are associated.

Methods For 24 AD patients and 18 controls [^{18}F]FDG and rs-fMRI data were available. [^{18}F]FDG standardized uptake values ratios (SUVr), with cerebellar gray matter as reference tissue, were calculated. Eigenvector centrality (EC) mapping was used to spatially analyze the functional brain network. Group differences were calculated for [^{18}F]FDG and ECM-values in 4 cortical regions (occipital, parietal, frontal and temporal) and across voxels, with age, gender and gray matter as covariates. Correlation of [^{18}F]FDG with ECM was calculated within groups.

Results Both lowered [^{18}F]FDG SUVr and EC values were seen in the parietal and occipital cortex of AD patients. However, [^{18}F]FDG yielded more robust and widespread brain areas affected in AD patients; hypometabolism was also observed in the temporal cortex and regions within frontal brain areas. Poor spatial overlap of both measures was observed. No associations were found between local [^{18}F]FDG SUVr and ECM.

Conclusion In conclusion, agreement of [^{18}F]FDG and ECM in AD patients seems moderate at best. [^{18}F]FDG was most accurate in distinguishing AD patients from controls.

Introduction

Neuronal dysfunction is of interest in AD, as it is occurs before neuronal loss and is thought to have a similar temporal pattern as cognitive decline [1]. Two methods have been widely used to investigate neuronal dysfunction in AD: 1) Positron emission tomography (PET) which measures glucose metabolism with Fluorine-18 labelled fluorodeoxyglucose [^{18}F]FDG; 2) Functional magnetic resonance imaging (fMRI), which measures blood oxygen level dependent (BOLD) contrast, to explore local neuronal dysfunction and functional connectivity between (remote) brain areas.

[^{18}F]FDG PET is useful in clinical practice [2]. With [^{18}F]FDG PET, reduced metabolism in the precuneus and bilateral parietal cortex [3,4], but also in frontal and parieto-temporal areas has frequently been observed in AD patients [5,6]. For rs-fMRI, patterns of co-varying activity in spatially distinct brain regions, referred to as functional connectivity [7,8], are believed to be more sensitive to disease state than simple measures of fMRI-BOLD complexity. Many studies have shown reduced functional connectivity in AD patients [9-12], particularly in precuneus and bilateral parietal cortex. As such, functional connectivity can provide an alternative method to [^{18}F]FDG PET for assessment of neuronal damage in AD. Several techniques can be used to examine functional connectivity. It has been shown that eigenvector centrality can easily be computed from rs-fMRI data [13] and that it is robust against global physiological effects [14]. Furthermore, eigenvector centrality mapping (ECM) does not require a-priori knowledge and provides voxel-wise information (similar to [^{18}F] FDG).

It has been shown that [^{18}F]FDG and rs-fMRI identify similar regions in AD and they are reported to be linked, although only a few studies have examined this association in AD patients directly [15-17]. If a strong connection exists, both methods could be interchangeable in AD. Using rs-fMRI instead of [^{18}F]FDG is less invasive and saves costs. A study by Drzezga et al. [15] found good spatial overlap of hypometabolism and lowered functional connectivity in MCI patients compared with controls in the precuneus, which was correlated across subjects. The authors reasoned that these findings support a causal mechanism between synaptic failure and functional disconnection. Other studies examining this association have focused mainly on functional connectivity of [^{18}F]FDG and its correspondence rs-fMRI functional connectivity [16,17].

The aim of this study was to investigate whether both imaging modalities provide similar information in AD patients. First, we will examine if similar brain regions are identified when comparing AD patients to controls using [^{18}F]FDG and ECM in 4 cortical regions (occipital, parietal, frontal and temporal) and in a voxelwise manner. Second we will examine the direct association between [^{18}F]FDG and ECM in a correlation analysis. It is expected that the precuneus and other parietal regions are identified with both [^{18}F]FDG and ECM and that associations are strongest within the, disease-affected, parietal cortex.

Materials and Methods

Participants

All participants underwent a standard dementia screening, which included a record of their medical history, neuropsychological testing, physical and neurological examinations, structural MRI and screening laboratory tests. Subjects represent a subset of individuals whose fMRI data and [^{11}C]PIB PET data were previously reported [18]. The combination of [^{18}F]FDG with fMRI data has not been reported earlier. Patients were excluded when they had a history of major psychiatric or neurological illness other than AD, used non-steroidal anti-inflammatory drugs, or showed clinically significant abnormalities other than AD on the MRI scan as determined by a neuroradiologist. The Mini Mental State Examination (MMSE) was part of neuropsychological testing [19]. Clinical diagnosis was established by a multidisciplinary team. Twenty-four patients were diagnosed with probable AD [20] and were compared with an elderly control group (n=18) who were recruited through advertisements of newspapers and underwent the same diagnostic procedure. Additional exclusion criteria for normal controls were subjective complaints, a history of major neurological or psychiatric illness, or abnormalities on the MRI scan. The study was approved by the Medical Ethics Review Committee of the VU University Medical Center. Ethics review criteria conformed to the Helsinki declaration. Written informed consent was obtained from subjects and/or subjects' caregivers after a complete written and verbal description of the study.

MR acquisition

MRI scans of all subjects were acquired using a 1.5 Tesla Sonata scanner (Siemens Medical Solutions, Erlangen, Germany). These scans included a coronal T1-weighted 3-dimensional magnetization-prepared rapid-acquisition gradient echo (MPRAGE) image (echo time 3.97 ms; repetition time 2,700 ms; inversion time 950 ms; flip angle 8°; 160 coronal slices; voxel size 1×1.5×1 mm^3) and resting state functional scans of 200 T2*-weighted echo planar imaging (EPI) volumes (TR=2850ms; TE=60ms; flip angle=90°; voxel size 3.3 mm isotropic). Subjects were instructed to lie still with their eyes closed and not to fall asleep during the resting state scan.

[^{18}F]FDG PET acquisition

[^{18}F]FDG scans were acquired using an ECAT EXACT HR+ scanner (Siemens/CTI, Knoxville, USA). The properties of this scanner have been reported elsewhere [21]. A head holder was used to restrict head movement, which was checked on a regular basis using external laser beams. For the [^{18}F]FDG scan, subjects rested for 10 minutes with their eyes closed in a dimly lit room with minimal background noise before [^{18}F]FDG was injected. Thirty-five minutes later, patients underwent a 10-minute transmission scan followed by a 15-minute (static) emission scan. Further details of [^{18}F]FDG scanning can be found elsewhere [22]. PET sinograms of both scans were corrected for dead time, tissue attenuation using the transmission scan, decay, scatter, and randoms. Next, images were reconstructed using a standard

filtered backprojection algorithm using a Hanning filter with a cut-off at 0.5 times the Nyquist frequency, resulting in a spatial resolution of 7 mm full width at half-maximum (FWHM) at the center of field of view [23]. A zoom factor of 2 and a matrix size of 256x256x63 resulted in a voxel size of 1.2x1.2x2.4 mm^3.

Structural MR analysis

All MRI analyses were performed using FMRIB Software (FSL 5.0.4 www.fmrib.ox.ac.uk/fsl) [24]. Non-brain tissue was removed from individual T1-images and segmented in gray matter (GM), white matter and cerebral spinal fluid. The GM probability maps were registered to standard space using non-linear registration. These images were averaged and flipped along the x-axis to create a symmetric, study specific GM-template. All native GM images were non-linearly registered to the template and subsequently corrected for local expansion or contraction [25].

fMRI analysis

Pre-processing in FSL included motion correction, spatial smoothing using a 7 mm Gaussian kernel to match the [^{18}F]FDG data, high-pass temporal filtering (0.01Hz), removal of non-brain tissue, and co-registration to standard space (MNI152) via the T1-weighted image. Eigenvector centrality was calculated using in-house fast-ECM software ([13]; github.com/amwink/bias/tree/master/matlab/fastECM). A mask of in-brain voxels across all subjects' fMRI data was calculated and applied before the EC maps were computed. This was done to since comparing the properties of different network topologies is a non-trivial problem. EC mapping does not require thresholding or binarizing of the connectivity matrix, so all subjects' networks had the same topology as well as the same size.

PET data analysis

Structural MRI T1-images were rigidly aligned to corresponding PET images using a mutual-information algorithm [26]. [^{18}F]FDG scans were analyzed using PVE-lab, a software program that makes use of a probability map based on 35 defined regions of interest (ROIs) [27]. Parametric images of standardized uptake value ratio (SUVr), using cerebellar gray matter as reference, were generated. Cerebellar glucose metabolism is relatively preserved in AD and, therefore, cerebellar gray matter was chosen as reference tissue for analysis. Partial volume effects could lead to an underestimation of [^{18}F]FDG SUVr [28]. However, correction using standard partial volume correction (PVC) methods is highly dependent on the actual method being used, as many uncertainties may affect accuracy and precision of (MRI based) partial volume corrections [29]. Therefore, PVC correction was not incorporated in the present study. Subjects' [^{18}F]FDG SUVr images were normalized to standard MNI152 2mm space using FLIRT (part of FSL; http://fsl.fmrib.ox.ac.uk/fsl/fslwiki/FLIRT) [30].

Group comparisons

All subsequent group comparisons and correlations were performed within the rs-fMRI mask described in section 2.5. Average [^{18}F]FDG SUVr and ECM values within the following 4 cortical ROIs were calculated: occipital cortex, parietal cortex, frontal cortex and temporal cortex, all based on the Harvard-Oxford cortical atlas (provided in FSL; http://www.cma.mgh.harvard.edu/fsl_atlas.html). This was performed for all subjects within subject specific GM voxels (thresholded at probability ≥0.5). Next, in order to assess differences in [^{18}F]FDG SUVr and ECM between groups on a voxel level, a non-parametric permutation test (5000 permutations) was used with voxel-wise GM probability maps, age and sex as covariates [31]. Family wise error (FWE) correction for multiple comparisons across space was performed, implementing threshold free cluster enhancement (TFCE) at $p<0.05$ [32]. Besides statistical tests, group difference maps were examined in order to understand voxel wise differences between AD patients and controls that did not survive the statistical threshold. To this end, group averages per voxel were calculated for AD patients and controls. Then, the average map for AD patients was subtracted from the average map for controls. To quantitatively assess the spatial similarity between changes in [^{18}F]FDG SUVr and ECM in AD patients versus controls, the Dice Similarity Coefficient (DSC) was calculated. The DSC measures overlap between two segmentations (A and B), and is defined as $DSC(A,B)= 2(A\cap B)/(A+B)$ where $\cap$ is the intersection [33]. A DSC of 0 represents no overlap and 1 represents perfect overlap.

Non-imaging statistics

All other statistical analyses were performed using SPSS (version 20.0; SPSS, Chicago, IL, USA). Age and MMSE score were compared between groups using an independent t-test. Distribution of gender between groups was compared using a Chi-square test. Mean [^{18}F]FDG SUVr and EC values in the 4 ROIs were compared between AD patients and controls with age and sex as covariates using ANCOVA. Pearson correlations of [^{18}F]FDG SUVr with ECM within the 4 ROIs were calculated within groups. Pearson correlations were calculated for [^{18}F]FDG SUVr and ECM values with MMSE score. Finally, receiver operating characteristics (ROC) curves, with regional [^{18}F]FDG SUVr and EC values in AD patients and controls were calculated. The area under the curve (AUC) was used to assess accuracy of both methods in distinguishing between AD patients and controls. A p-value below 0.05 was considered statistically significant.

Results

Combined [^{18}F]FDG and rs-fMRI data of 24 AD patients and 18 controls were available. As expected, MMSE scores were significantly lower in AD patients than in controls ($t(40)=11.09$, $p<0.01$). Age was also lower in AD patients ($t(40)=2.28$, $p<0.05$). An overview of demographic variables is given in Table 1.

Table 1; Subject characteristics

	Controls	AD patients	p-value
N	18	24	/
Age	66.56 ± 6.22	62.21 ± 6.05	0.03
Gender (M/F)	14/4	17/7	0.61
MMSE score	29.28 ± 0.58	23.50 ± 2.15	<0.01
Time between PET and MRI scan (days)	20.61 ± 24.64	15.42 ± 26.78	0.52
Mean [^{18}F]FDG SUVr in occipital cortex	0.97 ± 0.06	0.92 ± 0.07	0.04
Mean [^{18}F]FDG SUVr in parietal cortex	0.96 ± 0.07	0.87 ± 0.07	<0.01
Mean [^{18}F]FDG SUVr in frontal cortex	0.95 ± 0.07	0.93 ± 0.07	0.26
Mean [^{18}F]FDG SUVr in temporal cortex	0.85 ± 0.05	0.78 ± 0.05	<0.01
Mean EC-values in occipital cortex (*10000)	23.49 ± 0.55	23.14 ± 0.33	0.01
Mean EC-values in parietal cortex (*10000)	23.37 ± 0.28	23.21 ± 0.19	0.02
Mean EC-values in frontal cortex (*10000)	22.78 ± 0.20	22.89 ± 0.18	0.07
Mean EC-values in temporal cortex (*10000)	22.59 ± 0.26	22.66 ± 0.17	0.41

Data are presented as means ± standard deviations. Mean [18F]FDG SUVr and EC-values were corrected for age and sex. MMSE score = Mini mental state examination score (Folstein et al., 1983).

Regional [^{18}F]FDG and ECM in a group comparison

Mean [^{18}F]FDG SUVr in parietal ($p<0.01$), temporal ($p<0.01$) and occipital cortex ($p<0.05$) was significantly lower in AD patients when compared to controls. Mean EC values in occipital ($p<0.05$) and parietal cortex ($p<0.05$) were significantly lower in AD patients) (Table 1).

Voxel-wise [^{18}F]FDG and ECM in a group comparison

Significantly lower [^{18}F]FDG SUVr and EC values in AD patients compared to controls were observed (Figure 1). [^{18}F]FDG showed the largest group differences, with AD patients having lower [^{18}F]FDG SUVr in bilateral parietal cortex, precuneus, temporal cortex and small areas in bilateral occipital and medial frontal cortex. For ECM, lower EC values in AD patients were seen in left medial occipital cortex and left inferior temporal gyrus. The areas of [^{18}F]FDG SUVr and ECM identified in the group

comparison showed almost no overlap, which was confirmed by a DC of 0.01. Figure 1B shows the spatial overlap of lower [^{18}F]FDG SUVr and lower EC values in AD patients compared to controls when no statistical threshold was used (subtraction maps)d. Overlap was seen in several cortical areas and was most pronounced in parietal cortex, but also in superior temporal cortex and medial frontal regions. This spatial overlap corresponded to a DC of 0.58. For an overview of the number of voxels and the intersection see Table 2.

Figure 1; Significant results (FWE corrected p<0.05) of lowered [^{18}F]FDG SUVr (light blue) and lower ECM-values (blue) and the spatial overlap (yellow) in AD patients compared to elderly controls (A). Subtraction maps of decreased [^{18}F]FDG SUVr (light blue) and decreased ECM-values (blue) and the spatial overlap (yellow) in AD patients compared to controls (B). Results are displayed in radiological orientation on MNI 152 2mm template (x, y, z, coordinates: -46,-74,22). FWE: Family-wise error.

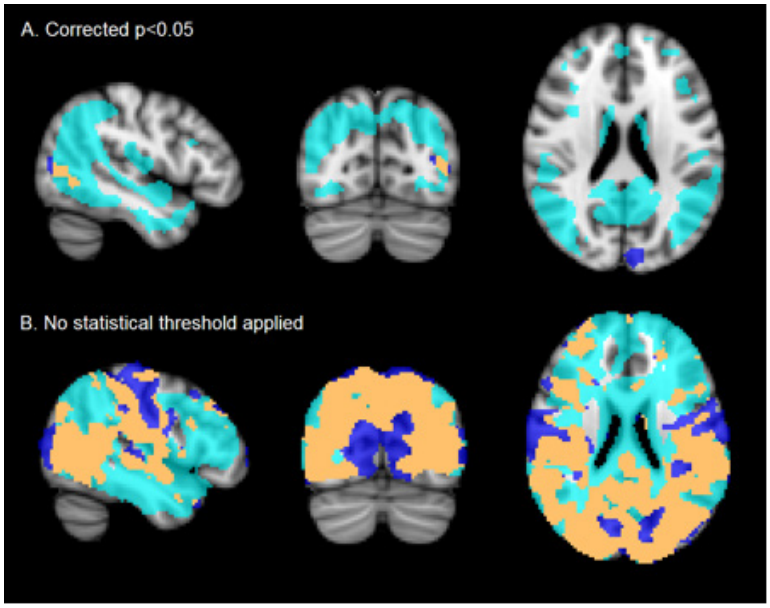

Table 2; Spatial overlap; Dice Similarity Coefficients and number of voxels of lowered [^{18}F]FDG SUVr and ECM-values in AD patients and the overlap.

	Dice Similarity Coefficient	# of voxels intersection	# of voxels [^{18}F] FDG	# of voxels ECM
T-test (FWE corrected p<0.05)	0.01	174	35304	664
Subtraction maps (no threshold)	0.58	63251	125617	93941

Total # voxels included was 194440.

Correlation of [^{18}F]FDG with ECM

No significant correlations between [^{18}F]FDG SUVr and ECM-values were found within the 4 cortical ROIs.

Correlation of [^{18}F]FDG and ECM with global cognitive performance

MMSE scores of healthy controls ranged from 28 to 30 and, because of this narrow range, were not included in this analysis. Neither [^{18}F]FDG SUVr nor EC values in the 4 ROIs showed a significant correlation with MMSE score in AD patients.

Receiver operating characteristics

ROC curves were calculated for [^{18}F]FDG SUVr in parietal and temporal cortex and for EC values in parietal and occipital cortex, i.e. the regions where strongest group differences were found (Figure 2). AUC was good for [^{18}F]FDG SUVr in parietal cortex (0.82), followed by [^{18}F]FDG SUVr in temporal cortex (0.80). Poor accuracy was found for EC values in both parietal (0.67) and occipital cortex (0.68).

Figure 2; Receiver operating characteristics (ROC) curves for mean [^{18}F]FDG SUVr in parietal and occipital cortex and for mean ECM-values in parietal and temporal cortex. AUC: Area under the curve (AUC). SUVr: Standardized uptake value.

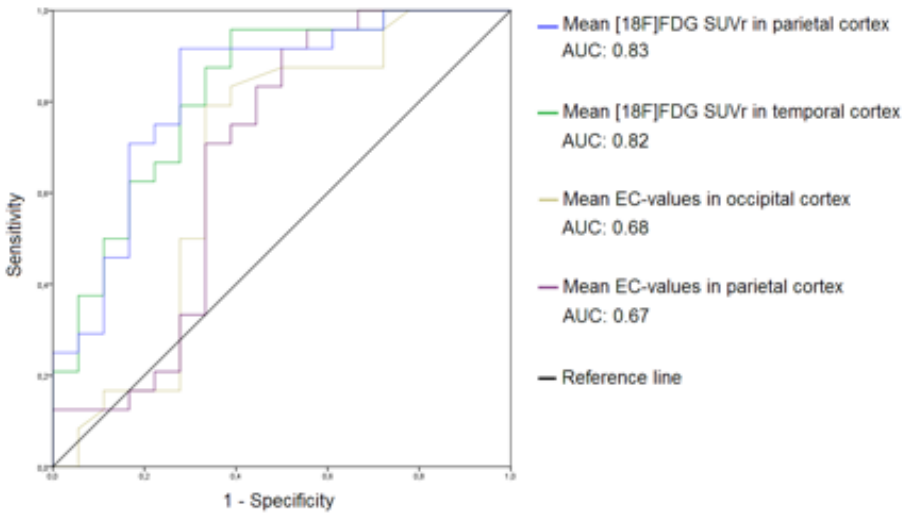

Discussion

The main finding of this study is that although [^{18}F]FDG and ECM both showed AD-related deficits in the parietal and occipital cortex, these techniques showed poor agreement in other cortical areas across the brain. Hypometabolism was more widespread than lowered centrality, including temporal cortex and small regions of the frontal cortex as well. In addition, no correlation between local [^{18}F]FDG SUVr and ECM was found.

Regions known to be susceptible to reduced metabolism in AD patients were replicated in both regional and voxel-wise analyses. Lower [^{18}F]FDG SUVr was seen in three of the four ROIs, i.e. parietal, occipital and temporal cortex. The voxel-wise analysis revealed more detail with lower [^{18}F]FDG SUVr in AD patients being found in bilateral parietal cortex, posterior cingulate cortex, precuneus, bilateral occipital cortex, medial frontal cortex and medial temporal areas, which is in line with previous research [4,5,15]. [^{18}F]FDG in the parietal cortex performed best in distinguishing AD patients from controls. This is in agreement with the clinical applicability of [^{18}F]FDG [2]. ECM, at present, does not seem suitable for clinical purposes. When examining group differences on a voxel-level with ECM, smaller regions compared to [^{18}F]FDG were identified; Lower centrality in AD patients was seen in occipital cortex, replicating previous findings from our group [34]. In the ROI analysis lowered EC values were found in 2 regions, i.e. occipital and in the parietal cortex. The occipital cortex together with the parietal cortex have been reported with highest centrality values for fMRI data in controls (14,34,35]. High centrality in the parietal/occipital cortex agrees with the role of these brain regions as hub within the healthy functional brain network; especially the precuneus has many connections to other brain regions, is energy demanding, and is important for information processing [15,36,37]. Interestingly, these highly connected, and energy demanding, brain regions seem most vulnerable in AD patients. High energy demands of hub regions may make these regions especially vulnerable to deficits in energy delivery [35]. Amyloid-plaque formation show a striking spatial overlap with the locations of cortical hubs [37]. It is commonly believed that accumulation of amyloid-β is followed by synaptic dysfunction, neuronal loss, and finally cognitive problems [1,38]. In contrast, results from transgenic mouse models indicate that neuronal activity might enhance amyloid-β deposition [39]. If so, measures of neuronal activity are promising for early detection of AD.

Even though the parietal and occipital cortex were identified with both techniques, spatial overlap of the regions identified in an voxel analysis with [^{18}F]FDG and ECM was very low. As described above, hypometabolism was more widespread than lowered centrality. In contrast, moderate spatial overlap (42%) of decreased functional connectivity and hypometabolism in MCI patients in the posterior cingulate cortex in MCI patients and controls has been reported earlier [15]. When examining simple subtraction maps, relatively good overlap (56%) of regions with lower metabolism and lower centrality in AD patients was found; Overlap was seen in the precuneus and posterior cingulate cortex, but also in occipital cortex and in

small regions of temporal and frontal areas. These results should be interpreted with caution since no statistical correction was performed. Besides group differences, the correlation of metabolism and centrality was investigated. We expected good associations for [^{18}F]FDG and ECM in disease-affected regions in AD patients, but no clear associations of [^{18}F]FDG SUVr with ECM were found. Drzezga et al. [15] found that hypometabolism *was* correlated with lower degree centrality in the precuneus across all subjects, but, similar to the present study, not within groups. Of course, centrality of a voxel within the whole-brain network is not the same as metabolism measured in a single voxel. Also, MCI patients represent the disease stage before AD. However, results from studies examining functional connectivity/centrality in AD are often related to metabolism changes since they are both believed to represent synaptic dysfunction [1]. In line with this hypothesis, Tomasi et al. [35] found that fMRI BOLD-signal amplitude, local and global degree centrality were correlated with glucose metabolism across healthy subjects. A recent paper of Di and Biswal [16] identified resting-state networks based on [^{18}F]FDG data and rs-fMRI data in elderly controls. The authors hypothesized that functionally connected regions would also show high correlations of metabolic activity. This hypothesis proved to be partially true; similar resting-state networks were identified with both measures, but anterior–posterior networks were absent for [^{18}F]FDG data. The discrepancy between [^{18}F]FDG and functional connectivity was reasoned to reflect the difference in coupling of energy consumption and ongoing neural synchronization within the RSNs [16]. This fits the results of our study; centrality (neural synchronization) and metabolism (energy consumption) were not correlated in AD patients and elderly controls. The two methods might therefore provide complementary information [17], and possibly reflect changes at different timepoints in the disease course of AD. The combination of methods could possibly be useful in improving early clinical diagnosis of AD. Future research should focus on conversion to AD in elderly subjects and MCI patients.

Limitations

The extent to which centrality was affected in AD patients on a voxel-level was less pronounced than in the regional analysis. Possibly this can be attributed to differences in inherent spatial smoothness of the data [40]. In order to account for these spatial differences for the two techniques, preprocessing of rs-fMRI data included smoothing with a relative large kernel of 7mm FWHM in order to match the [^{18}F]FDG data. After normalization of [^{18}F]FDG data to standard MNI space, average intrinsic smoothness of the data was FWHMx, FWHMy, FWHMz: (10x12x11mm). This was somewhat smaller for ECM after normalization (10x11x11mm), but closest to [^{18}F]FDG. To illustrate, when applying a commonly used smoothing factor of 5mm FWHM on rs-fMRI data, intrinsic smoothness was 8x8x8mm. Furthermore, gray matter loss in AD patients could have influenced measures of metabolism and rs-fMRI. No correction for partial volume effects was applied, since no perfect solution exist [29]. Finally, ECM is a relative new measure of connectivity in AD research, which has certain advantages [14]. Studies examining other measures of functional connectivity could provide more insight into the association of metabolism with functional connectivity in AD.

Conclusion

Hypometabolism and lowered centrality in AD patients was observed in occipital and parietal cortex. However, agreement in other cortical regions was absent. In addition, the direct association of [^{18}F]FDG and ECM was very weak. Both methods are therefore believed to represent different mechanisms in healthy elderly and AD patients. [^{18}F]FDG SUVr in the parietal cortex was best in distinguishing between AD patients and controls and is useful in clinical practice, whereas ECM, at present, does not seem to be suitable for clinical purposes.

References

[1] Jack CR Jr, Knopman DS, Jagust WJ, Petersen RC, Weiner MW, Aisen PS, et al. 2013. Tracking pathophysiological processes in Alzheimer's disease: an updated hypothetical model of dynamic biomarkers. Lancet Neurol 12:207-216.

[2] Silverman DH, Small GW, Chang CY, Lu CS, Kung De Aburto MA, Chen W, et al. 2001. Positron emission tomography in evaluation of dementia: Regional brain metabolism and long-term outcome. JAMA 286(17):2120-7.

[3] Chetelat G, Desgranges B, Eustache F. 2006. Brain profile of hypometabolism in early Alzheimer's disease: relationships with cognitive deficits and atrophy. Rev Neurol [Paris] 162:945-951.

[4] Li Y, Rinne JO, Mosconi L, Pirraglia E, Rusinek H, DeSanti S, et al. 2008. Regional analysis of FDG and PIB-PET images in normal aging, mild cognitive impairment, and Alzheimer's disease. Eur J Nucl Med Mol Imaging 35:2169-2181.

[5] Mosconi L, Sorbi S, de Leon MJ, Li Y, Nacmias B, Myoung PS, et al. 2006. Hypometabolism exceeds atrophy in presymptomatic early-onset familial Alzheimer's disease. J Nucl Med 47:1778-1786.

[6] Dukart J, Mueller K, Villringer A, Kherif F, Draganski B, Frackowiak R, et al. 2013. Relationship between imaging biomarkers, age, progression and symptom severity in Alzheimer's disease. Neuroimage Clin 3:84-94.

[7] Biswal BB, Mennes M, Zuo XN, et al., 2010. Toward discovery science of human brain function. Proc Natl Acad Sci USA 107:4734-4739.

[8] Bassett D, Bullmore E, Verchinski B, Mattay V, Weinberger D, Meyer-Lindenberg A (2008) Hierarchical organization of human cortical networks in health and schizophrenia. J Neurosci 28:9239–9248.

[9] Damoiseaux JS, Prater KE, Miller BL, Greicius MD (2006): Functional connectivity tracks clinical deterioration in Alzheimer's disease. Neurobiology of Aging 33 (2012) 828.e19–828.e30

[10] Greicius MD, Srivastava G, Reiss AL, Menon V (2004): Defaultmode network activity distinguishes Alzheimer's disease from healthy aging: Evidence from functional MRI. Proc Natl Acad Sci USA 101:4637-4642.

[11] Rombouts SA, Damoiseaux JS, Goekoop R, Barkhof F, Scheltens P, Smith SM, Beckmann CF (2009): Model-free group analysis shows altered BOLD fMRI networks in dementia. Hum Brain Mapp 30:256–266.

[12] Binnewijzend MAA, Schoonheim MM, Sanz-Arigita E, Wink AM, van der Flier WM, Tolboom N. 2011. Resting-state fMRI changes in Alzheimer's disease and mild cognitive impairment. Neurobiol Aging 33(9):2018-2028.

[13] Wink AM, de Munck JC, van der Werf YD, van den Heuvel OA, Barkhof F 2012. Fast eigenvector centrality mapping of voxel-wise connectivity in functional magnetic resonance imaging: implementation, validation, and interpretation. Brain Connect 2:265-274.

[14] Lohmann G, Margulies DS, Horstmann A, Pleger B, Lepsien J, Goldhahn D, et al. 2010. Eigenvector centrality mapping for analyzing connectivity patterns in fMRI data of the human brain. PLoS One 5: e10232.

[15] Drzezga A, Becker JA, Van Dijk KR, Sreenivasan A, Talukdar T, Sullivan C, et al. 2011. Neuronal dysfunction and disconnection of cortical hubs in non-demented subjects with elevated amyloid burden. Brain 134:1635-1646.

[16] Di X, Biswal BB. 2012. Alzheimer's disease neuroimaging initiative. Metabolic brain covariant networks as revealed by FDG-PET with reference to resting-state fMRI networks.

Brain Connect 2(5):275-283.

[17] Wehrl HF, Hossain M, Lankes K, Liu C, Bezrukov I, Martirosian P, et al. 2013. Simultaneous PET-MRI reveals brain function in activated and resting state on metabolic, hemodynamic and multiple temporal scales. Nat Med 19(9):1184-1189.

[18] Adriaanse SM, Sanz-Arigita EJ, Binnewijzend MA, Ossenkoppele R, Tolboom N, van Assema DM, Wink AM, Boellaard R, Yaqub M, Windhorst AD, van der Flier WM, Scheltens P, Lammertsma AA, Rombouts SA, Barkhof F, van Berckel BN (2014): Amyloid and its association with default network integrity in Alzheimer's disease. Hum Brain Mapp; Mar;35(3):779-91. doi: 10.1002/hbm.22213. Epub 2012 Dec 14.

[19] Folstein MF, Robins LN, Helzer JE. 1983. The Mini-Mental State Examination. Arch Gen Psychiatry 40:812.

[20] McKhann GM, Knopman DS, Chertkow H, Hyman BT, Jack CR Jr, Kawas CH, et al. 2011. The diagnosis of dementia due to Alzheimer's disease: recommendations from the National Institute on Aging-Alzheimer's Association workgroups on diagnostic guidelines for Alzheimer's disease. Alzheimers Dement 7:263-269.

[21] Brix G, Zaers J, Adam LE, Bellemann ME, Ostertag H, Trojan H, et al. 1997. Performance evaluation of a whole-body PET scanner using the NEMA protocol. National Electrical Manufacturers Association. J Nucl Med 38:1614-1623.

[22] Ossenkoppele R, Tolboom N, Foster-Dingley JC, Adriaanse SF, Boellaard R, Yaqub M, et al. 2012. Longitudinal imaging of Alzheimer pathology using [11C]PIB, [18F]FDDNP and [18F] FDG PET. Eur J Nucl Med Mol Imaging 39:990-1000.

[23] Boellaard R, van Lingen A, Lammertsma AA (2001): Experimental and clinical evaluation of iterative reconstruction (OSEM) in dynamic PET: Quantitative characteristics and effects on kinetic modelling. J Nucl Med 42:808–817.

[24] Smith SM, Jenkinson M, Woolrich MW, Beckmann CF, Behrens TE, Johansen-Berg H, et al. 2004. Advances in functional and structural MR image analysis and implementation as FSL. Neuroimage 23:Suppl 1:S208-19, S208-S219.

[25] Douaud G, Smith S, Jenkinson M, Behrens T, Johansen-Berg H, Vickers J, James S, Voets N, Watkins K, Matthews PM, James A (2007): Anatomically related grey and white matter abnormalities in adolescent-onset schizophrenia. Brain 130:2375-2386.

[26] Maes F, Collignon A, Vandermeulen D, Marchal G, Sueens P. 1997. Multimodality image registration by maximization of mutual information. IEEE Trans Med Imaging 16:187-198.

[27] Svarer C, Madsen K, Hasselbalch SG, Pinborg LH, Haugbøl S, Frøkjaer VG, et al. 2005. MR-based automatic delineation of volumes of interest in human brain PET images using probability maps. Neuroimage 24:969-979.

[28] Fazio F, Perani D (2000): Importance of partial-volume correction in brain PET studies. J Nucl Med 41:1849–1850.

[29] Nissen IA, Boellaard R, Ossenkoppele R et al (2012): Impact of partial volume corrections on quantitative brain PET studies [abstract]. SNM Conference 2012.

[30] Jenkinson M, Bannister P, Brady JM, Smith SM. 2002. Improved Optimisation for the Robust and Accurate Linear Registration and Motion Correction of Brain Images. NeuroImage 17(2):825-841.

[31] Nichols TE, Holmes AP (2002): Nonparametric permutation tests for functional neuroimaging: A primer with examples. Hum Brain Mapp 15:1-25.

[32] Smith SM, Nichols TE (2009): Threshold-free cluster enhancement: Addressing problems of smoothing, threshold dependence and localisation in cluster inference. Neuroimage 44:83-98.

[33] Zou KH, Warfield SK, Bharatha A, Tempany CM, Kaus MR, Haker SJ, et al. 2004. Statistical

validation of image segmentation quality based on a spatial overlap index. Acad Radiol 11:178-189.

[34] Binnewijzend MA, Adriaanse SM, Van der Flier WM, Teunissen CE, de Munck JC, Stam J, Scheltens P, van Berckel BN, Barkhof F, Wink AM (2014): Brain network alterations in Alzheimer's disease measured by eigenvector centrality in fMRI are related to cognition and CSF biomarkers. Hum Brain Mapp; May;35(5):2383-93. doi: 10.1002/hbm.22335

[35] Tomasi D, Wang GJ, Volkow ND, 2013. Energetic cost of brain functional connectivity. PNAS:110(33):13642-13647.

[36] de Haan W, van der Flier WM, Wang H, Van Mieghem PF, Scheltens P, Stam CJ (2012): Disruption of functional brain networks in Alzheimer's disease: What can we learn from graph spectral analysis of resting-state magnetoencephalography? Brain Connect 2:45-55.

[37] Buckner RL, Sepulcre J, Talukdar T, Krienen FM, Liu H, Hedden T, Andrews-Hanna JR, Sperling RA, Johnson KA (2009): Cortical hubs revealed by intrinsic functional connectivity: Mapping, assessment of stability, and relation to Alzheimer's disease. J Neurosci 29:1860-1873.

[38] Hardy J, Selkoe DJ. 2002. The amyloid hypothesis of Alzheimer's disease: progress and problems on the road to therapeutics. Science 297:353-356.

[39] Cirrito JR, Kang JE, Lee J, Stewart FR, Verges DK, Silverio LM, Bu G, Mennerick S, Holtzman DM (2008): Endocytosis is required for synaptic activity-dependent release of amyloid-_ in vivo. Neuron 58:42–51.

[40] Radua J, Canales-Rodríguez EJ,Pomarol-Clotet E, Salvador R. 2014. Validity of modulation and optimal settings for advanced voxel-based morphometry. Neuroimage 86:81-90.